CCFE
CULHAM CENTRE FOR FUSION ENERGY

UK Atomic Energy Authority

UKAEA-CCFE-PR(25)299

A. M. Patel, R. Barnsley

2-Axis goniometer facility for x-ray characterisation of diffractors

2-Axis goniometer facility for x-ray characterisation of diffractors

A. M. Patel, R. Barnsley

This is a preprint of a paper submitted for publication in
Review of Scientific Instruments

2-Axis goniometer facility for x-ray characterisation of diffractors

A. M. Patel[†]

United Kingdom Atomic Energy Authority, Culham Campus, Abingdon, Oxfordshire, OX14 3DB, UK

Details of a 2-axis goniometer used with an x-ray source are presented, including measurements of double-crystal integrated reflectivity of diffractors used in spectrometers at JET. Polarization corrections of the measurements are calculated for estimates of the single-crystal integrated reflectivity. Synchronised parallel and dispersive diffractor motion profiles at this facility have good angular error distributions that involve all motors of ∼2 arcsec over a complete range of the accessible Bragg angles (0 - 86°).

[†]Electronic address: ash.patel@ukaea.uk

INTRODUCTION

The study of impurity line-radiation and continua forms an integral part of our understanding of the tokamak plasma. Impurity species can impact detrimentally e.g. fuel ion dilution of the plasma bulk and radiative power-losses through radiation. They may range from Be to Cu and heavier elements such as W depending upon the confinement device internal structure. Their absolute concentrations can be most easily deduced from the study of their one- and two-electron ion emissions. This is because of their relatively simple term-scheme compared with multi-electron systems. In general terms they are relatively bright intensities, well-resolved and lie in the 1-15Å x-ray wavelength range. Commonly used diffractors include mineral crystals and synthetic multilayer mirrors (MLM). They offer advantages of superior reflectivity though inferior diffraction widths - especially MLMs - above ∼30Å compared with grating techniques, however emissions of interest are usually well isolated in the spectral neighbourhood [1].

OVERVIEW

This paper centres on the measurement of x-ray diffractor properties. One technique is to illuminate them with an extended x-ray vacuum anode source to simulate the plasma [2, 3], however the source spectral bandwidth is to some extent indeterminate due to the presence of the background continuum. The approach described here adopts the two-crystal reflection technique: measurements in the parallel non-dispersive configuration, (1,-1) mode, the two-crystal diffraction profile or "rocking curve" is independent of the profile of the source spectrum or the vertical or horizontal beam divergence [4]. This is because the two crystals are aligned such that their diffraction planes are parallel, ensuring that the wavelength selected by the first crystal is identically reflected by the second crystal. This configuration maintains a fixed geometric relationship where the Bragg condition for a specific wavelength is satisfied simultaneously by both crystals, regardless of the spectral distribution of the source. We use a near-point source with x-rays excited from selected metals and alloys. In the technique employed here, the first diffractor provides near monochromatic illumination of the second diffractor whose integrated reflection efficiency is independent of the source bandwidth as long as the diffractor properties are unchanged over small Bragg angles ($\delta\theta_B \sim 0.1°$). The facility consists of an x-ray source and a goniometer that is referenced in [5] in general terms. We complement the description with detailed system performance and results presented for the diffractor batch used in spectrometers that study x-rays from the JET D-T plasma (DTE2 and DTE3 campaigns [6]) and other physics campaigns over the last two decades [7].
The goniometer utilises motor technology which is capable of achieving resolution and repeatability of 1.27/2 arcsec, however the study of diffractors with instrument widths below about 8 arcsec is not pursued in this report. This is due to the errors in overall synchronised angular movement.

DESIGN AND CONFIGURATION

Generalised source and diffractor orientations, movement configurations and a hardware photo are shown in FIG.1. FIG. 1(a-d) schematically shows the possible source and diffractor configurations. Parallel diffractor movement, "rocking curve" or the (1,-1) mode, is shown in FIG. 1(a,c), whereby the diffractor characteristics are measured, while the dispersive (1,1) mode, FIG. 1(b,d), analyses the source spectral intensity. FIG. 1(c,d) shows a fixed source which is the design adopted here. Alternating the second diffractor between these modes ($\pi - 2\theta_B$)

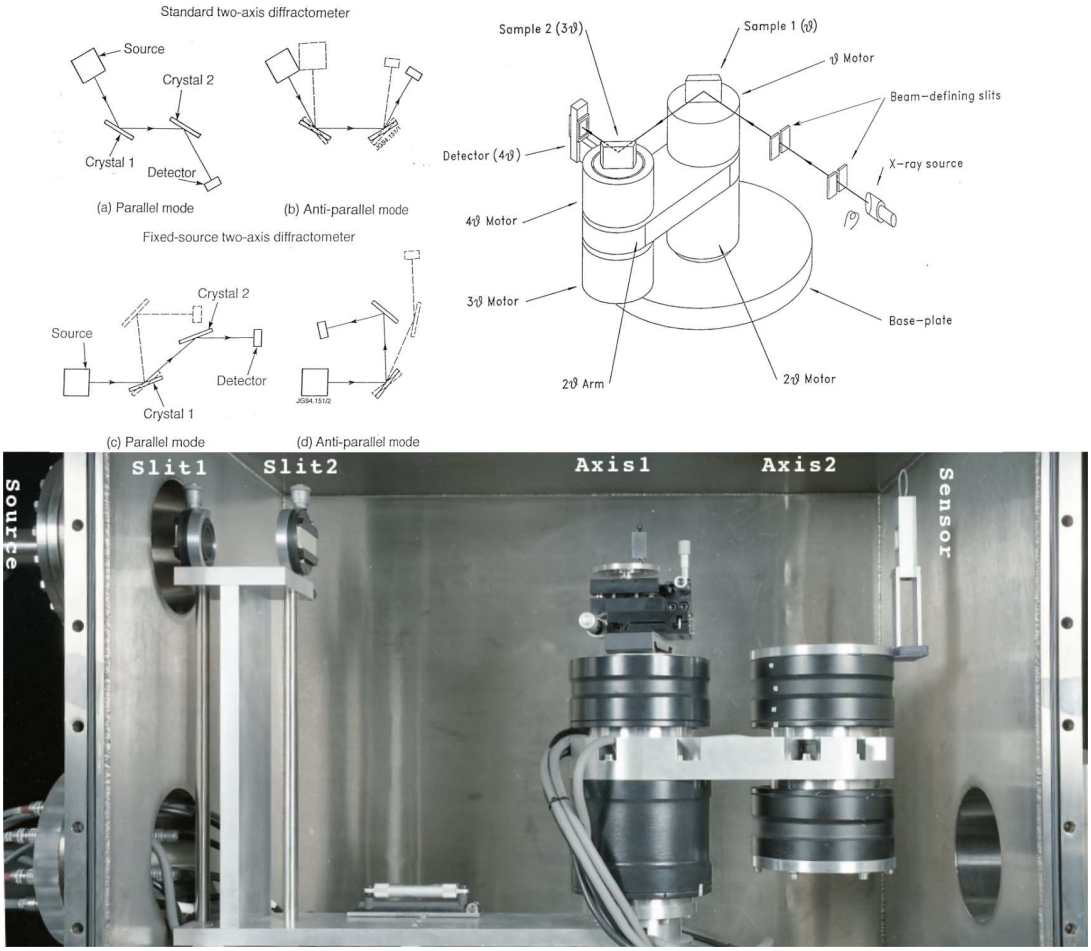

FIG. 1: Schematic layout (a-d) illustrates possibilities of source and double diffractor combinations. Modes of operation can have fixed diffractor (a, b) or a fixed source/primary diffractor axes (c, d). The second diagram shows our adoption of a fixed source, collimating slits and an unrestricted primary diffractor rotation about Axis1. Axis2 has an orbiting gas-proportional sensor all of which rotate about Axis1. The picture shows partial hardware layout consisting of fine tilt and rotation adjustment mechanisms for the primary diffractor. The slits, motors and detector are shown along with some cabling and vacuum feed-throughs for motor control, temperature sensors, interlocks and gas-proportional operation (bias-voltage, gas piping, charge-amplifier, DC voltages). Source is located at the left of the vacuum chamber.

yields the lattice-spacing parameter, 2d. The "rocking curve" measures the diffraction profile at a given order for known wavelengths corresponding to the principal anode K-, L- and M- inner-shell radiation from the source. Both the double-crystal reflectivity R_{cc} and the 2d are hence measured. The source spectrum profile and vertical and horizontal beam divergence independence in the (1,-1) mode is satisfied here as the beam collimation, defined by the slits, is better than 0.2°.

It is not possible to derive the single-crystal profile directly from the (1,-1) measurements due to the symmetrical nature of the parallel configuration, also the diffraction profile of many diffractors is typically asymmetrical. The first crystal partially polarizes the radiation to the second diffractor, so the contributions from the π and σ components cannot be separated out by this technique. However, in the case of two identical crystals, as in the work here, at the same diffraction order, R_{cc} is related to the single-crystal diffraction integral, R_c, by

$$R_{cc} = 2R_c \frac{1 + k_\theta^2}{(1 + k_\theta)^2}$$

where the polarization ratio, $k_\theta = R_{c\pi}/R_{c\sigma}$, depends on diffractor properties: absorption, extinction and defect density. Limiting cases are based on Darwin theory [8]: for a perfect crystal with zero absorption $k_p = |cos(2\theta_B)|$, and, for a mosaic crystal $k_m = cos^2 2\theta_B$, real diffractors lie within these limits. To illustrate this FIG. 2 shows integrated reflectivities based on the Darwin-Prins formulation [4] of the theory of Bragg reflection for perfect crystals with absorption for ADP101. Corrections applied to R_{cc} are highest at $\theta_B = 45°$, with a maximum

error of ∼30% near the Bragg angles of 35° and 55°.

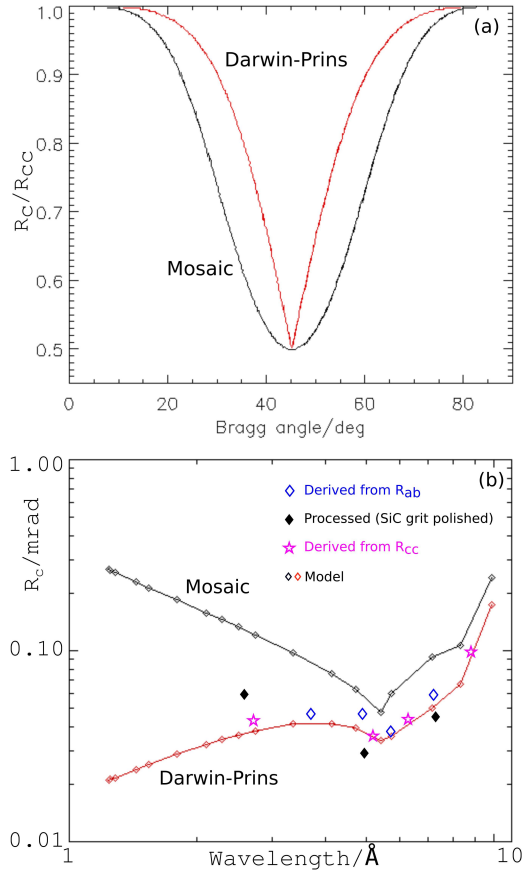

FIG. 2: (a) Relationship between the one- and two-reflection integrals as a function of Bragg angle for the k_p and k_m limits, and (b) Model estimate of R_c specifically for the ADP101 diffractor, also shown for comparison are some measurements from [9] where the R_{ab} measurements are made in the (1,1) mode.

Goniometer motion and control

The whole facility is in a controlled thermal environment which maintains the diffractor temperature in the range 17-19 °C; crystal temperatures reported here are within the range 18±0.2 °C. Each diffractor is mounted and located such that the light facing surface has 3 surface contacts, each of which has dimensions of 1x3mm, the axis of each is rotated by direct drive brushless servo motors which are clean-room compliant and compatible with operating at the vacuum levels achieved here (∼10^{-5}mbar); encoder-motor operate in closed-loop which ensures absolute position control and repeatability during synchronised motion of diffractors. The motors (Parker Inc. Dynaserv DM series, 6", 20Nm torque, 1.265 arcsec encoder resolution, FIG. 3 photo) have high torque and good resolution incremental encoders. The closed-loop operation ensures that the motor current is minimal during profile moves and when at rest: this is key to greater system temperature control. Typical goniometer position error distributions of the complete system is as shown in FIG. 3 over a (1,-1) motion profile at low and high movement speeds. The errors are well within full width half maximum of the diffractors studied here and are taken into account in the analysis and curve-fitting post acquisition. A single-anode gas-

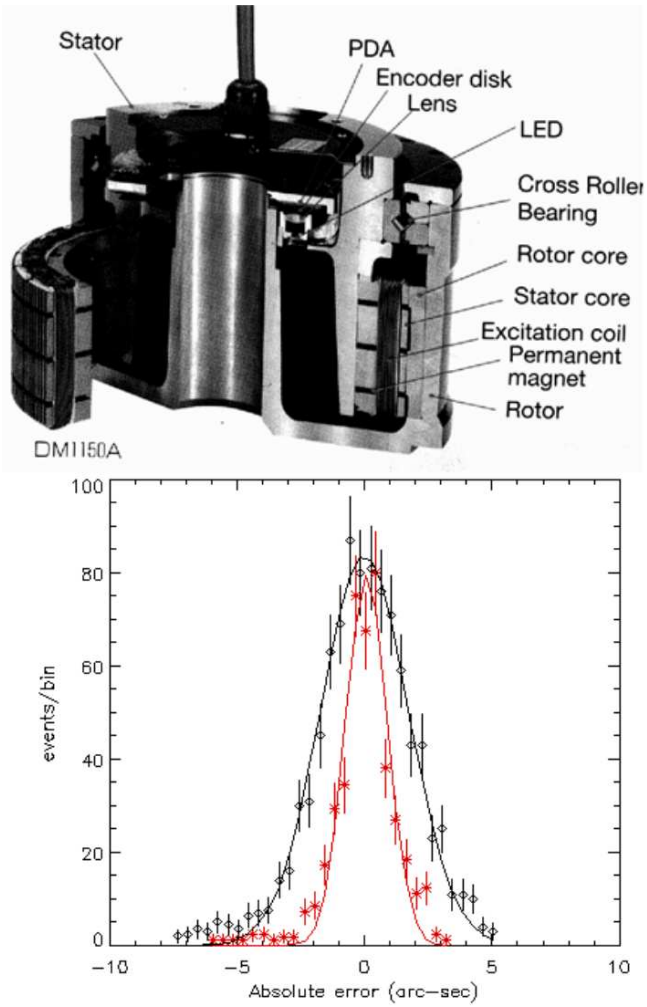

FIG. 3: Detail: brushless servo motor with a built-in encoder. Also shown are absolute errors during $\delta\theta_B \sim$ 10/120 arcsec/s rotation speed movement profile, FWHM are ≈2/3.75 arcsec respectively.

proportional detector is used, its width ultimately limits the Bragg-angle illumination of the diffractors to the range 0 - 86°. The detector is windowed on two opposite sides with aluminised 2μm Mylar. The sensitive part of the sensor is more than twenty times the slit width: hence a large proportion of the diffracted radiation is collected. FIG. 4(a) shows relative sensitivity of the sensor to narrow beam of W-M_α radiation as it is scanned across the window: spatial variations over this angle

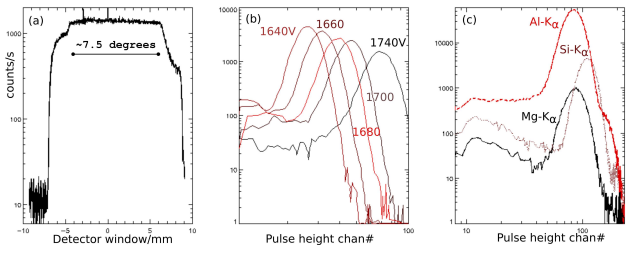

FIG. 4: Detector characteristics: (a) across the window (W-M_α, 50μm width), (b) detector pulse-height response to applied voltage bias (T*l*AP, 1.7kV/10mA source potential, 150s scan time,), and (c) Element-resolved K_α PHA from an Al-alloy anode (T*l*AP, 6kV/2.5mA, 190s scan time).

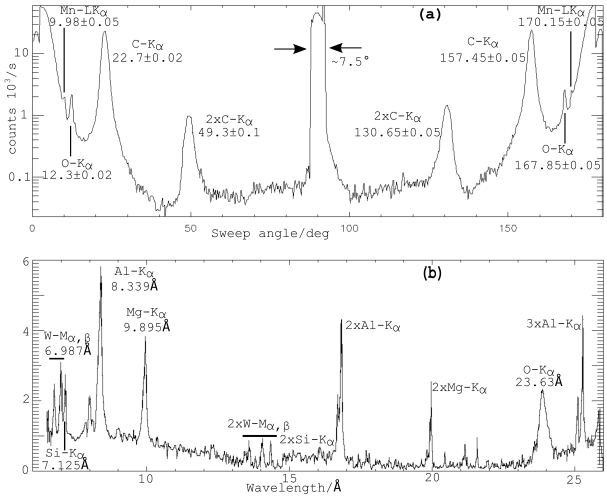

FIG. 5: Typical single diffractor sweeps: (a) full, 0< θ_B <180° OV117 multilayer, central 7.5° bright signal corresponds to direct detector illumination, and (b) complete spectral survey of T*l*AP (0-26Å, 0< θ_B <86°).

range (∼7.5°) are small: within peak counting statistics (< 2.5%). A custom built charge-sensitive preamplifier (5V/pC charge-gain) is housed within the sensor which uses standard P10 gas mixture (10%CH_4/Ar) at 1 atmosphere pressure. Necessary gas piping, high-voltage anode bias, low-voltage pre-amplifier supply voltages, temperature sensors, movement interlocks, motor and encoder cabling are so arranged that free and uninterrupted rotation is allowed along the whole of the dispersive plane. The pulse-height response is detailed in FIG. 4(b,c) as a function of the bias voltage and at different x-ray energies corresponding to various anode materials is also shown. Pulse-height discrimination capability is useful e.g. when order-isolation is required. Motion profile software and acquisition triggering are by traditional means: CAMAC-based high count rate multi-channel latching scalar records raw (noise-discriminated) and multiple amplitude-thresholded detector counts along with encoder data.

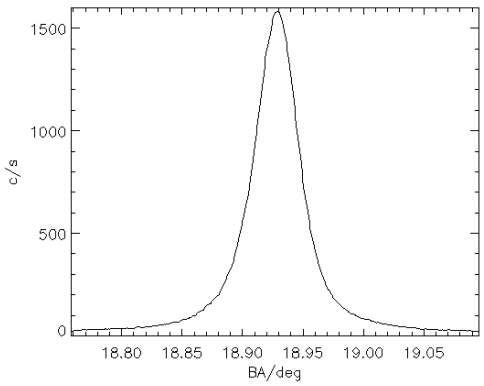

FIG. 6: T*l*AP rocking curve of Al-K_α (8.3376Å). The FWHM determined from curve fitting is 147.3 ± 1.6 arcsec.

X-ray source

An externally rotatable, liquid cooled, triple anode source is composed of pre-selected elements which emit characteristic principal inner-shell light of interest [10]. Rapid anode change is facilitated by a separate valved vacuum system which may be let up to atmospheric pressure, changed and pumped to workable pressures within short periods of time. Up to 500W of continuous power is the limit of the anode and liquid-cooling system which exceeds the maximum power-supply delivery parameters (10kV/30mA). Vacuum is maintained in a nominal oil vapour-free pressure by a turbo-molecular pump and vacuum oil-mist filter system. Collimation along the plane of dispersion is controlled by two modified 3mm thick copper slits (Rank-Hilger Monospek 1000, Hilger Analytical, Westwood, Margate CT9 4JL, UK) with throughput angle range ±15 arcsec - 15 arcmin with vertical stops to define diffractor sub-illumination if so required, nominal slit throughput here is ±6 arcmin in the dispersive plane.

I. RESULTS, DISCUSSION

An example of a complete 180° single-crystal scan of a multilayer mirror is shown in FIG. 5(a) (Ovonyx multilayer systems, Rigaku Holdings Corp. Matsubara-cho 3-9-12, Akishima, Tokyo T198-8666, Japan). Carbon, oxygen and manganese emissions - the anode constituents - can be measured up to two orders.

Over the survey at the sweep angle position of 0° the source/diffractor/sensor are all in-line, at θ_B ∼90° the ordering is source/sensor/diffractor. As the sweep continues the Bragg angle decreases from 90° to 0°. In-between

Anode	λ Å	θ_B °	2d Å	Width arcsec	P_{cc} %	R_{cc} 10^{-4}rad	R_c est 10^{-4}rad	DP R_c 10^{-4}rad
T*l*AP (1,-1)								
W-M_β	6.757	15.234	25.715	55	27.8	2.33	2.25-2.32	2.3-3.3
Al-K_α	8.339	18.924	25.710	147	27.1	2.61	2.49-2.56	2.3-3.3
Al-K_α*	8.34			161	26.9	2.73	2.64-2.65	
Zn-L_α*	12.25			276	15.8	3.06	2.42	
Cu-L_β	13.053	31.230	25.707	155	12.8	3.04	2.20-2.60	2.1-2.28
Cu-L_α	13.336	31.230	25.720	168	12.3	3.15	2.22-2.70	2.1-2.28
Ni-L_α#	14.56			220				
T*l*AP (2,-2)								
Mo-L_α	2.751	12.139	26.165	39	47.2	0.29	0.27-0.28	
Ag-L_α	4.12	18.926	25.404	75	22.1	0.25	0.24-0.25	
W-M_α	6.983	32.86	25.74	25.4	11.3	0.44	0.38-0.31	
Si-K_α	7.1	33.619	25.647	26	11.1	0.44	0.37-0.29	
Al-K_α	8.34	40.388	25.742	40	9.4	0.56	0.37-0.30	
Mg-K_α	9.89	50.213	25.74	58	6.7	0.58	0.39-0.31	
OV44 (1,-1)								
Fe-L_α	17.59	23.66	43.925	860	6.6	8.9	7.83-8.63	∼13.30
Mn-L_α	19.45	26.288	43.915	920	5.7	8	6.60-7.60	∼7.00
O-K_α	23.62	32.589	43.923	1200	4.55	8.2	5.49-7.05	∼11.50
OV117 (1,-1)								
O-K_α	23.2	12.23	110.0	1080	4.4	8.00	7.80-7.92	
C-K_α	44.7	22.81	115.1	2200	11.9	39.4	35-38.2	
B-K_α	67.6	36.2	114.5	6055	10.8	100	60-78	

TABLE I: Summary of measured parameters for T*l*AP (over two orders) and OV44/OV117 multilayer mirrors: double-crystal width, peak reflectivity (P_{cc}) and integrated reflectivity (R_{cc}). Other measurements are also included for comparison (*[11], #[3]). The polarization-corrected range of the integrated reflectivity (R_c) for each diffractor is also shown. Darwin-Prins model calculations (DP R_c) are also shown as a guide where possible.

the two sweeps the detector obstructs the light at over 7.5° sweep range which defines the maximum θ_B ∼86°.
Multilayer mirrors, generally, have wider instrument widths (FIG. 5(a)) compared with other lower 2d diffractors - FIG. 5(b) is an example of this: complete Bragg angle sweep for T*l*AP (2d≈25.9Å, Al-alloy anode as source), the abscissa is now wavelength, this time up to three orders of some lines can be measured.
A detailed "rocking curve" example (1,-1) is shown in FIG. 6 of the Al-K_α radiation showing good signal:noise response and source stability over the scan period (∼600s). Indeed the source intensity is stable to a high degree over time (e.g. over a full Bragg-angle sweep) as the source voltage/anode current is maintained within a good tolerance by the power-supply units.
Repeating the (1,-1) motion profiles over a multitude of wavelengths, diffractors and orders, the resulting errors from curve fits over data are summarised in TABLE I. Measured R_{cc}, derived R_c, lattice-spacing, peak reflectivity, FWHM are shown. Also polarization-corrected calculations, yielding the range of R_c are included where possible. Historical measurements from [3] and [11] are also shown in TABLE I for comparison purposes, however these diffractors do not constitute the batch presented here though they do however show broad agreement with measurements here.
The multilayers perform well from a reflectivity perspective but with wider instrument widths as expected. Estimated R_c errors vary from a few % (T*l*AP) to ∼15% for the multilayers - these errors will propagate through to absolute line or continua measurements from the tokamak plasma. The R_c estimates are consistent with model-based calculations and errors.
These results are important for the calculation of absolute intensities of plasma emissions from JET, which will eventually enable plasma-impurity concentration estimates.
Further application of this approach to the study of e.g. the impact of radiation and neutron damage from D-T burning plasma reactors on diffractor properties is envisaged.

ACKNOWLEDGMENTS

The author would like to thank R. Barnsley, N. J. Peacock and N. C. Hawkes for technical contributions. This work has been funded by the EPSRC Energy Programme [grant number EP/W006839/1]. To obtain further information on the data and models underlying this paper

please contact PublicationsManager@ukaea.uk.

REFERENCES

[1] N. Peacock, R. Barnsley, K. Lawson, I. Melnick, M. O'Mullane, M. Singleton, and A. Patel, Review of scientific instruments **68**(4), 1734 (1997).

[2] H. Morsi, H. Röhr, and U. Schumacher, Zeitschrift für Naturforschung A **42**(10), 1051 (1987).

[3] R. Barnsley, U. Schumacher, E. Källne, H. Morsi, and G. Rupprecht, Review of scientific instruments **62**(4), 889 (1991).

[4] A. H. Compton and S. K. Allison, *X-rays in theory and experiment* (Macmillan and Co., Ltd., London, 1935).

[5] N. Peacock, R. Barnsley, A. Patel, M. O'Mullane, M. Singleton, and J. Ashall, Review of scientific instruments **66**(2), 1175 (1995).

[6] C. F. Maggi, Nuclear Fusion (2023).

[7] R. Barnsley, J. Brzozowski, I. Coffey, K. Lawson, A. Patel, T. Patel, N. Peacock, and U. Schumacher, Review of scientific instruments **63**(10), 5023 (1992).

[8] C. G. Darwin, The London, Edinburgh, and Dublin Philosophical Magazine and Journal of Science **27**(158), 315 (1914).

[9] R. Hall, *A quantitative description of Bragg analysers* (University of Leicester (United Kingdom), 1980).

[10] A. C. Thompson, D. Vaughan, *et al.*, *X-ray data booklet*, vol. 8 (Lawrence Berkeley National Laboratory, University of California Berkeley, CA, 2001).

[11] M. Lewis, *A quantitative treatment of Bragg diffraction.*, Ph.D. thesis, University of Leicester (1982).